Mechanical Systems and Signal Processing 115 (2019) 469–482

Contents lists available at ScienceDirect

Mechanical Systems and Signal Processing

journal homepage: www.elsevier.com/locate/ymssp

Experimental study of the variations in the electromechanical properties of piezoelectric energy harvesters and their impact on the frequency response function

Patricio Peralta [a,c], Rafael O. Ruiz [b,c,*], Viviana Meruane [a]

[a] Department of Mechanical Engineering, Universidad de Chile, Beauchef 851, Santiago, Chile
[b] Department of Civil Engineering, Universidad de Chile, Blanco Encalada 2002, Santiago, Chile
[c] Uncertainty Quantification Group, Center for Modern Computational Engineering, Facultad de Ciencias Físicas y Matemáticas, Universidad de Chile, Beauchef 851, Santiago, Chile

ARTICLE INFO

Article history:
Received 10 October 2017
Received in revised form 9 April 2018
Accepted 1 June 2018
Available online 15 June 2018

Keywords:
Uncertainty quantification
Piezoelectric energy harvesters
Experimental validation

ABSTRACT

This work presents a comprehensive study of the uncertainties involved in the Frequency Response Function (FRF) of Piezoelectric Energy Harvesters (PEHs) based on experimental results. A proper experimental setup is designed facilitating the FRF identification for different PEHs. The test protocol consists in three test that quantify the aleatoric and epistemic uncertainties by the study of repeated measurements, variation in the mounting process, and variations in the electromechanical properties of the materials employed in the harvester. The experimental setup and the test protocol are tested employing two different bimorph-type harvesters identified as Model A and B. 20 harvesters corresponding to Model A and 10 to Model B are tested multiples times under the test protocol proposed. Results clearly indicate that the most important source of uncertainties deals with the variability of the electromechanical properties of the PEH, which is particularly greater than: (i) the noise on the measurements, (ii) the variations introduced by the clamping condition, and (iii) the dimensional variations in the geometry. The results are also compared with predictions performed by adopting a recent numerical framework to propagate uncertainties in PEHs. The present work is particularly important since it presents the experimental evidence of the variations in the electromechanical properties of PEH and their influence on the FRF. Additionally, the results not only validate the uncertainty propagation procedures previously proposed but also suggest that their use is mandatory to estimate the FRF. This work presents, to the best of the authors' knowledge, the first effort to experimentally quantify the uncertainties in PEHs.

1. Introduction

The piezoelectric energy harvesting from vibratory environments has been widely studied in the last decade. The devices usually employed to this purpose consist in cantilevered beams composed by a series of alternate layers of piezoelectric and elastic materials. Depending on the number of piezoelectric layers, the harvesters typically receive the name of unimorph or

* Corresponding author at: Department of Civil Engineering, Universidad de Chile, Chile
E-mail address: rafaelruiz@uchile.cl (R.O. Ruiz).

https://doi.org/10.1016/j.ymssp.2018.06.002
0888-3270/

bimorph. The unimorph type corresponds to a single piezoelectric layer bonded to another layer that acts as support (usually referred as substructure layer) while the bimorph type consists in a substructure layer bonded to two piezoelectric layers, one at each side [1]. The energy harvesting is achieved by the deformation of the cantilevered beam induced by the vibratory environment (direct piezoelectric effect [1]). Since these devices offer high electrical power density, they become particular interesting to low-power electronics, especially for remote sensor applications [2].

Along the recent years, the researchers have been trying to model the Piezoelectric Energy Harvester (PEH) behaviour in detail. In general, the most relevant advances seem to go in particular directions: (1) proposing of adequate electromechanical coupling models [3–5], (2) optimization of PEHs for broad-band vibratory processes [6,7], (3) push the technology to a Micro-electro-mechanical systems (MEMS) [8,9] [10], and (4) development of efficient circuitry [11]. In that sense, the adequate modelling of PEH plays a determinant role for their prediction, optimization and design. Several models have been developed, but in particular two of them have been widely accepted and used in the scientific community: the analytical distributed parameter solution introduced by Erturk and Inman [4,12] and the finite element plate model introduced by De Marqui Junior et al. [13]. These models are particularly interesting since they have been ample tested showing an important level of accuracy.

Although the models available offer a good description of the physics involved in PEH, its accuracy relies in the complete knowledge of the electromechanical properties of the piezoelectric material together the geometrical characteristics of the harvester. In a recent work, Franco and Varoto [14] presented a design framework for PEHs but taking into account the uncertainties related to the geometrical parameters and the load resistance of the harvester. The results revealed that the incorporation of these uncertainties affects significantly the prediction of the PEH. On the other hand, Ruiz and Meruane [15] observed that the manufacturers typically report these electromechanical properties with variations close to ±20% of their nominal values. In that sense, the authors proposed a procedure to propagate these variations (all obtained from the literature) in order to identify the expected Frequency Response Function (FRF) and its corresponding confidence interval. The work conducted by Ruiz and Meruane presents one of the first efforts to describe the dynamic behaviour of PEHs assuming the electromechanical characteristic as uncertain parameters. As a result, the authors conclude that in order to obtain more robust predictions is mandatory to account the characteristic of the PEH as uncertain parameters or improve the manufacturing tolerance to decrease the variability in the PEH parameters. In other words, the accuracy in the prediction of the well-known deterministic models will be lost if the information related to the characteristic of the PEH is omitted. However, the study performed by the authors was conducted only through simulation; no experiments were performed at the time. Despite the extensive description of the effect of the uncertainties in the FRF of PEHs, there is still the need to perform an experimental characterization of these uncertainties. In particular, several questions are still open, e.g., how different really are the FRFs of many theoretically identical PEHs? Is it that difference greater than the repeatability error of one PEH? Is it really the nominal prediction as bad as the one anticipated (based on the available information about the variability of the electromechanical properties) by procedure presented by Ruiz and Meruane?

The work presented here specifically answers the previous questions by addressing the experimental characterization of the uncertainties in PEHs. A fair comparison between the variability obtained theoretically and by the experimental results requires a significant amount of measurements of different harvesters. For instance, it would be necessary to dispose and identify (experimentally) the FRF of a large number of harvesters (all of them having the same nominal values). Afterwards, the experimental dispersion of the FRF could be compared with the estimation offered theoretically by [15]. Note that the experimental measurement of only one harvester does not offer any relevant information for a validation since there is no information on how representative of the whole group is the harvester chosen. In that sense, the main contribution of this research deals with: (a) the design of a test protocol to quantify uncertainties in PEH; (b) the experimental identification of the uncertainty associated to the repeatability, imperfect mounting, and manufacturing process; and (c) the validation of the theoretical model for uncertainty propagation in PEHs proposed previously in [15].

2. Experimental procedure

2.1. Experimental setup

The experimental identification of the FRF in PEHs requires the direct measurement of the base acceleration together with the voltage generated by the piezoelectric layer. Then, the goal of the experimental setup is to find a configuration that allows the imposition of a controlled base excitation while the respective measurements are performed. The excitation is imposed by the use of an electromagnetic shaker, which requires an amplifier that can be controlled from a computer. The computer and the amplifier are connected by a data module that serves as signal generator and data processing unit (data acquisition). The PEH is attached to the electromagnetic shaker in such a way that a cantilevered condition is enforced (the clamp consists in two pieces joined by screws). The accelerometer is mounted on the top of the PEH base and its signal is sent to the data module. The voltage generated in the PEH is also sent to the data module to be analysed. Fig. 1 shows a picture of the experimental setup while Fig. 2 is a companion scheme for the clamped end of the PEH. Note that a proper mounting (Fig. 2) is designed to facilitate the installation and uninstallation of the PEH, the cantilever condition is obtained by locating the extreme of the PEH inside a socket where two bolts are tightened to clamp the harvester.

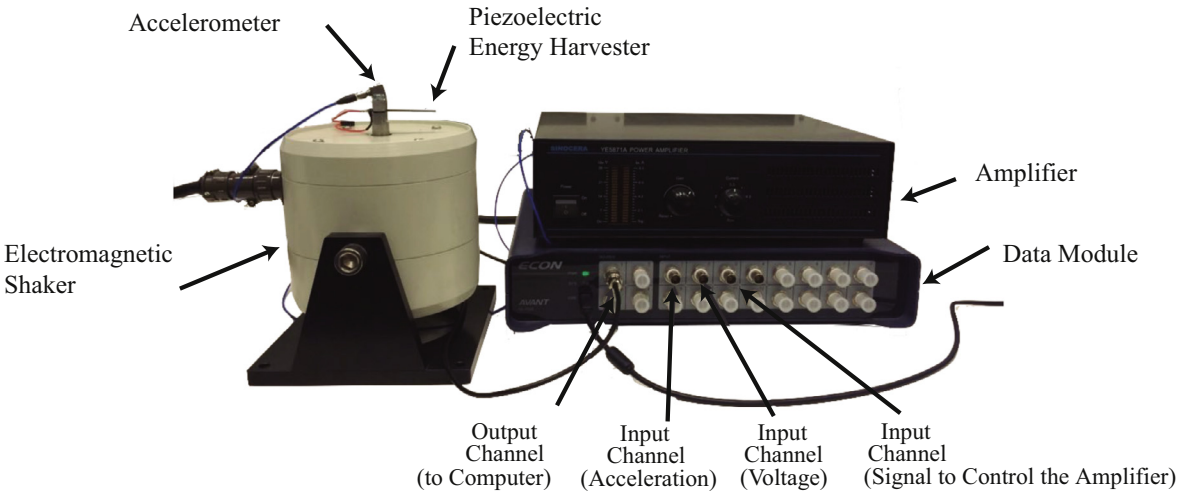

Fig. 1. Experimental setup for the identification of FRFs.

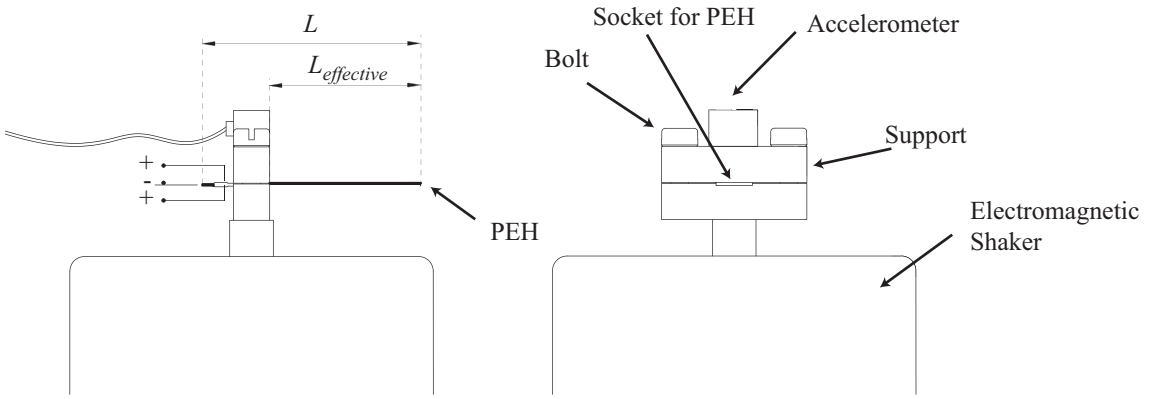

Fig. 2. Details of the PEH mounting.

The shaker has a frequency range of 10 Hz–4 kHz, a maximum acceleration of 400 m/s^2, and a vibration amplitude range of ±5 mm. It can be configured to execute signals commonly used in dynamic analysis of structures, e.g., harmonic, white noise, sweep, impulse, among others. The accelerometer employed to record the base acceleration has a sensitivity equal to 100 mV/(m/s^2). The generated voltage, as response to the excitation, is measured in a simple electric circuit made up of the PEH and an electrical resistance of 1000 ± 50 [Ω]. The data module has four output channels, sixteen input channels, 96.000 Hz of maximal sampling frequency and a setup software that controls the data acquisition and processing. Two different commercial PEHs are studied, both corresponding to bimorphs with layers of piezoelectric material (ZT-5X45) attached to a substructure of carbon fibre. The geometrical parameters and material properties are listed in Table 1.

Table 1
Nominal characteristics of the PEH tested. The manufacturer indicates that electromechanical properties reported here can exhibit a variation of ± 20% [16].

	Model A	Model B
Density substructure ρ_s	Not Available	Not Available
Young's Modulus Substructure E_s	Not Available	Not Available
Elastic Compliance PZT s_{11}^E	16.4×10^{-12} m^2 N^{-1}	16.4×10^{-12} m^2 N^{-1}
PZT Strain Constant d_{31}	-320×10^{-12}C N^{-1}	-320×10^{-12}C N^{-1}
Permittivity ϵ_{33}^T	$4500 \times (8.854 \times 10^{-12})$ F m^{-1}	$4500 \times (8.854 \times 10^{-12})$ F m^{-1}
Density PZT ρ_p	7.4×10^3 kg m^{-3}	7.4×10^3 kg m^{-3}
Length L	40 mm	60 mm
Width b	10 mm	10 mm
Total thickness $2h_p + h_s$	0.8 mm	0.8 mm

As the goal of this research is to study the uncertainties in PEHs, it is required to identify the FRFs of various harvesters with the same nominal characteristics. In that sense, 20 and 10 PEHs of models A and B, respectively, are disposed to be tested. Each harvester is identified with a number and a letter in the following format PZT-letter-number, the letter indicates whether the PEH corresponds to Model A or B, while the number serve as an individual identification, for example, PZT-A-05 corresponds to the fifth PEH of Model A.

The length, width and total thickness of all tested harvesters are verified with a micrometer (precision of 0.001 mm). The mean and standard deviation of those geometric characteristics are presented in Table 2. Here, it is possible to observe small coefficients of variation (lower than 2.6%), indicating an important level of precision in the manufacturing process associated to the external dimensioning of the PEH. The variability found here is in agreement with the values previously reported in the literature, by example in [15]. However, it is notorious that the mean value of the thickness obtained from measurements differs from the nominal value reported in Table 1 (differences close to 10%). This difference is relevant since the thickness belongs to the set of parameters that affects the most the variability of the FRF [15], thus it is expected differences between the recorded and the nominally predicted FRF.

2.2. Experimental identification of FRFs

The FRF can be estimated by measuring the excitation and the vibration response of the PEH. For this particular case, the excitation corresponds to the acceleration at the base of the PEH, while the response corresponds to the output voltage or the output electrical power. The experimental setup allows imposing any given excitation, e.g. pure harmonic, frequency sweep, white noise, pulse-like accelerations, or any other prescribed form defined by a function. Given the input (acceleration at the base) and output (voltage generated) time-histories, the FRF can be calculated as follows:

$$H(i\omega) = \frac{V(i\omega)}{\ddot{U}_g(i\omega)} \tag{1}$$

where $\ddot{U}_g(i\omega)$ and $V(i\omega)$ corresponds to the Fourier Transform of the acceleration at the base and the output voltage, respectively. However, it is decided to employ the following alternative formulation which allows smoother results in the presence of noise:

$$H(i\omega) = \frac{S_{V\,\ddot{U}_g}}{S_{\ddot{U}_g\,\ddot{U}_g}} \tag{2}$$

here, $S_{\ddot{U}_g\,\ddot{U}_g}$ stands for the Power Spectral Density (PSD) of the input acceleration while $S_{V\,\ddot{U}_g}$ stands for the Cross Spectral Density of the output voltage and the input acceleration.

In order to establish a test procedure, four different excitations are imposed: white noise, pulse-like excitation, pure harmonic and a frequency sweep. Fig. 3 presents the experimental identification of the FRFs for two PEHs (single sample of Model A and another of Model B) employing the mentioned excitations. Results present the frequency sweep as the best option in terms of noise level, number of data in frequency domain, and time to perform measurements. Therefore, it is decided to keep the frequency sweep as excitation for all the tests conducted. Note that the FRF identified by applying the frequency sweep could be considered noise-free. In particular, the noise introduced by the sensors in the measurement of the output voltage and the input acceleration are almost 3 order of magnitudes lower than the values recorded in the interested range of frequencies. The assumption of a noise-free FRF identification (by employing sweep excitations) is evidenced in Fig. 3 since the black curve presents a continuous and smooth behaviour over the frequency range studied.

After defining the excitation strategy, i.e., imposing a sweep frequency excitation; it is necessary to adopt some criteria to set the excitation amplitude (acceleration amplitude imposed by the shaker at the base of the PEH). In this regard, the FRF is identified applying the same sweep frequency function, but imposing different acceleration amplitudes, the results are presented in Fig. 4 for both PEH models used in this work. Results clearly indicates a nonlinear behaviour for acceleration amplitudes greater than 0.04 m/s^2 since the FRF significantly changes its shape, maximum value and natural frequency. In general, the maximum value and fundamental natural frequency reported in the FRF decrease for increments in the excitation amplitude above 0.04 m/s^2. This trend has been described previously by other authors [17–19]. However, the importance to conduct this analysis relies on the identification of the acceleration threshold to enforce a linear behaviour rather than to

Table 2
Geometric characteristics measured for all PEHs studied. Mean values and coefficient of variations (in parenthesis) are reported.

	Model A	Model B
Length L	40.012 mm (0.2%)	60.046 mm (0.1%)
Width b	10.028 mm (0.3%)	10.064 mm (0.1%)
Thickness h_s	0.201 mm (0.2%)	0.201 mm (0.2%)
Total thickness $2h_p + h_s$	0.730 mm (1.2%)	0.713 mm (2.6%)

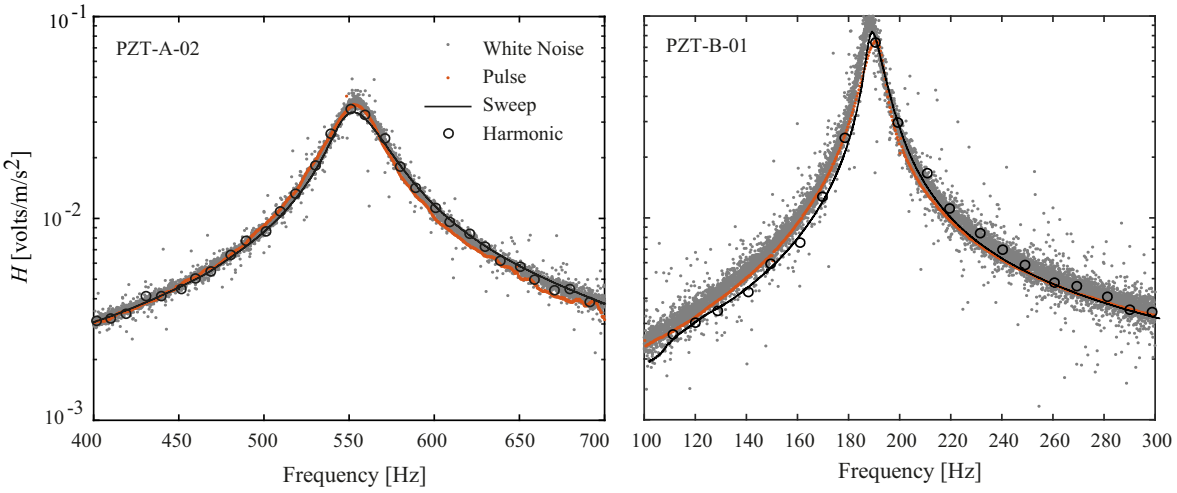

Fig. 3. FRF identified with different excitations, left figure corresponds to Model A and right figure to Model B.

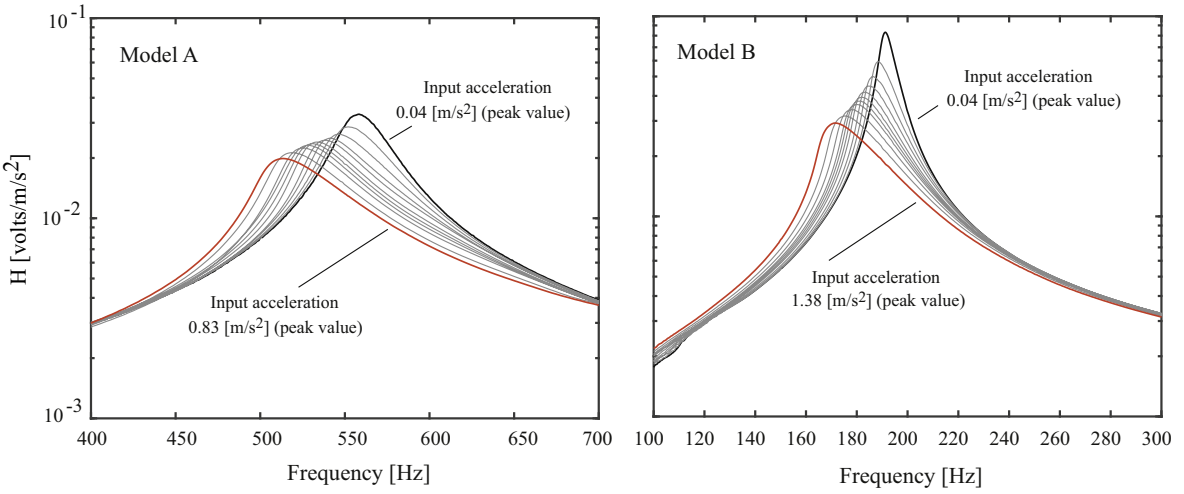

Fig. 4. Experimental response of the PEHs under large excitation amplitudes.

characterize the nonlinear performance. In Fig. 4, two limit FRFs are identified: (1) the red solid line that corresponds to the FRF for the maximum acceleration amplitude imposed before inducing a permanent damage in the PEH and (2) the black solid line that corresponds to the linear FRF. Note that input accelerations with amplitudes lower than 0.04 m/s^2 lead to the FRF presented in black solid lines. The minimum acceleration that the electromagnetic shaker can control is about 0.001 m/s^2, which is 40 times lower than the maximum acceleration employed to guarantee a linear behaviour. Note that even in this case the instrumental noise could be neglected. Finally, it is decided to set the acceleration amplitude equal to 0.04 m/s^2 for all test conducted in order to impose the greater acceleration to guarantee a linear behaviour.

The proposed procedure to identify the uncertainties in PEHs relies in three tests. The first test (Test 1), identifies the basal variations presented in the experiment. The FRF of each PEH is identified multiple times in order to evaluate how consistent are the measurements. This analysis allows the quantification of the basal level of uncertainty. Test 2, evaluates the change in the FRF when a PEH is removed from the shaker and reinstalled again. The test helps to identify how relevant is the installation process in the FRF estimation, especially when it is compared with the basal level of variations. The last test (Test 3) is focused on the FRF identification of PEHs that are nominally identical. Here, it is possible to compare the FRF variations due to basal condition, installation process and variability on the material properties. Furthermore, the results can be compared with the predicted variations obtained adopting a proper uncertainty propagation technique, which is described in the following section.

3. Numerical model to estimate uncertainties in FRFs

The procedure presented by Ruiz and Meruane [15] is employed to quantify the expected uncertainties in the FRF. Here, the well-known prediction model proposed by Erturk and Inman in 2008 [4,12] is used in companion with a stochastic technique based on Monte Carlo Simulation to estimate the variability of the FRF due to variations in the characteristics of the PEH (geometric parameters and electromechanical properties). As the procedure relies on two different stages: (1) the adoption of a deterministic predictor, and (2) the use of this predictor to propagate uncertainties related to the characteristics of the PEH; it is considered necessary to offer some insights on these issues to facilitate future implementations.

3.1. Deterministic predictor of the FRF in PEH

First, it is necessary to establish a deterministic model to identify the FRF of the PEH. In this particular case, the FRF is obtained by employing the methodology presented in [12], such that the frequency response of the output voltage per unit of the base acceleration can be expressed as an explicit formula that depends on the base acceleration frequency Ω and a vector $\boldsymbol{\theta}$ containing the characteristics of the PEH. In particular, the vector $\boldsymbol{\theta}$ is composed by: the length L, the width b, the thickness of the piezoelectric layer h_p, the thickness of the substructure layer h_s, the piezoelectric density ρ_p, the substructure density ρ_s, the substructure elastic modulus E_s, the damping ratio ζ, the elastic compliance at constant electric field s_{11}^E, the piezoelectric strain constant d_{31}, and the permittivity at constant stress ε_{33}^T. From now on, the FRF is denoted as $H(\boldsymbol{\theta},\Omega)$ to explicitly indicate the dependency on the characteristic of the PEH and its excitation frequency. Following the procedure presented in [15], $H(\boldsymbol{\theta},\Omega)$ could be expressed as:

$$H(\boldsymbol{\theta},\Omega) = \left(\frac{i\Omega}{i\Omega + k_{pzt}}\boldsymbol{\varphi}\right)\left[-\mathbf{I}\Omega^2 + i\Omega\mathbf{C}_{eq} + \mathbf{K}_{eq} + \frac{1}{i\Omega + k_{pzt}}\boldsymbol{\chi}\boldsymbol{\varphi}^T\right]^{-1}\mathbf{r} \tag{3}$$

Eq. (3) is obtained by arranging the analytical solution proposed by Erturk and Inman in [12]. The analytical solution is obtained by adopting a modal expansion of M eigenfunctions of an Euler-Bernoulli beam composed by layers of different materials (piezoelectric materials and other materials typically employed as structural support in PEHs). Here, i corresponds to the imaginary unit; k_{pzt} contains the electrical characteristics of the harvester as the electric resistance and the piezoelectric layer capacitance; while $\mathbf{I}$, $\mathbf{C}_{eq}$, and $\mathbf{K}_{eq}$ are M−by−M matrices corresponding to the identity, damping, and stiffness matrices, respectively. $\boldsymbol{\varphi}$, $\boldsymbol{\chi}$, and $\mathbf{r}$ are column vectors representing the mechanical coupling, the electrical coupling, and the mechanical forcing amplification due to the inertial effect. Ultimately, all these parameters could be related to the PEH characteristics $\boldsymbol{\theta}$ following the procedure presented in Appendix A. Furthermore, Eq. (3) corresponds to a traditional deterministic approach widely employed in the dynamic characterization of PEH [15], i.e., the predictor have been validated by other researchers to describe the dynamic behaviour of PEH in conditions that could be considered free of uncertainties. After fully described the deterministic predictive model, the question that arises is related to how to use this model to propagate the uncertainties usually found in the PEH characteristics. To answer this question and perform the required task, a stochastic sampling method is applied over the deterministic predictor such that the variability of the FRF could be accounted, details are offered next.

3.2. Stochastic prediction of the FRF

Here, the goal is to estimate the variation of the FRF due to variations on the vector $\boldsymbol{\theta}$. In that sense, the model parameter vector $\boldsymbol{\theta}$ can be modelled as a random vector defined by the PDF identified as $p(\boldsymbol{\theta})$. These uncertainties are propagated such that the expected value of the FRF can be estimated by solving the following probabilistic integral:

$$E[H|\Omega] = \int_{\Theta} H(\boldsymbol{\theta},\Omega)p(\boldsymbol{\theta})d\boldsymbol{\theta} \tag{4}$$

In this equation, $E[H|\Omega]$ corresponds to the expected FRF for a given excitation frequency after propagating the uncertainties in $\boldsymbol{\theta}$. Please note that $H(\boldsymbol{\theta},\Omega)$ is a determinist estimator thus it is independent of the uncertainty model $p(\boldsymbol{\theta})$. Contrary, $E[H|\Omega]$ exclusively depends on $p(\boldsymbol{\theta})$. Also, it is important to remark that Eq. (4) only quantifies the uncertainties due to the variation of $\boldsymbol{\theta}$. Another source of uncertainties (by example the basal uncertainties) could be introduced as an additive error e modifying Eq. (4) as $E[H|\Omega] = \int (H(\boldsymbol{\theta},\Omega) + e)p(\boldsymbol{\theta})p(e)d\boldsymbol{\theta}de$. However it is decided not to include this additive error since there is no prior information about the error and its probabilistic model $p(e)$.

Additionally, it is possible to identified the probability P_o that H exceed a certain value $H_{threshold:}$

$$P(H > H_{theshold}|\Omega) = P_o \tag{5}$$

The latter equation is given by a probabilistic integral such that:

$$P[H > H_{theshold}|\Omega] = \int_{\Theta} I_F(\boldsymbol{\theta},\Omega)p(\boldsymbol{\theta})d\boldsymbol{\theta} \tag{6}$$

where the indication function $I_F(\boldsymbol{\theta},\Omega)$ is equal to zero if $H \leqslant H_{theshold}$ and equal to one if $H > H_{theshold}$.

There are different procedures to solve Eqs. (4) and (6), being the stochastic simulation one of the most commonly procedure adopted, which is the scheme used in the present work, specifically the Monte Carlo Importance Sampling technique. The base of the method is to drawn a set of samples $\{\boldsymbol{\theta}_j,\ j=1,\ldots,K\}$ from a proposal density $q(\boldsymbol{\theta})$ to estimate the probabilistic integral presented in Eq. (4) as

$$E[H|\Omega] \approx \frac{1}{K}\sum_{j=1}^{K}\frac{H(\boldsymbol{\theta}_j,\Omega)p(\boldsymbol{\theta}_j)}{q(\boldsymbol{\theta}_j)} \tag{7}$$

It is possible to show that the optimal proposal density $q(\boldsymbol{\theta})$ is a PDF proportional to the integrand of Eq. (4). However, the method also yields a good approximation if $q(\boldsymbol{\theta})$ is chosen such that its peak is near to the global maximum of the integrand, and has a spread larger than that of $p(\boldsymbol{\theta})$. A common implementation of this procedure is realized in a standard Gaussian space (a space transformation is required), then the proposal density is chosen as a multivariate Gaussian PDF centred in the integrand of Eq. (4) (which has to be expressed in the standard Gaussian space) with a covariance matrix equal to the identity. Specific computational details on this procedure could be found in [20,21]. The precision of the importance sampling method to estimate the probabilistic integral in Eq. (4) can be evaluated by computing the variance of the estimator (Eq. (7)). In this sense, the following expression for the coefficient of variation of the estimator gives information about the adequate number of samples employed.

$$\delta_{estimator} = \frac{1}{\sqrt{K}}\frac{\sqrt{\frac{1}{K}\sum_{j=1}^{K}\left(\frac{H(\boldsymbol{\theta}_j,\Omega)p(\boldsymbol{\theta}_j)}{q(\boldsymbol{\theta}_j)}\right)^2-\left(\frac{1}{K}\sum j=1^{K}\frac{H(\boldsymbol{\theta}_j,\Omega)p(\boldsymbol{\theta}_j)}{q(\boldsymbol{\theta}_j)}\right)^2}}{\frac{1}{K}\sum_{j=1}^{K}\frac{H(\boldsymbol{\theta}_j,\Omega)p(\boldsymbol{\theta}_j)}{q(\boldsymbol{\theta}_j)}} \tag{8}$$

Finally, the idea is to choose a number of samples K such that $\delta_{estimator}$ be lower than certain level. In particular, the number of samples used in this work is 10.000, given a $\delta_{estimator}$ lower than 0.05 (or 5%) for all configurations of PEHs studied. Additionally, it should be noted that Eq. (6) could be solved adopting the same procedure but replacing $H(\boldsymbol{\theta}_j,\Omega)$ by $I_F(\boldsymbol{\theta},\Omega)$ in Eq. (7).

The probabilistic integral presented in Eq. (4) corresponds to the expected value of the FRF for a given excitation frequency Ω. Then, to identify the FRF for a wide range of frequencies it is necessary to recursively evaluate the Eq. (4) at the interest frequencies. In order to establish a consistent estimation error, it is decided to employ the same set of samples $\{\boldsymbol{\theta}_j,\ j=1,\ldots,K\}$ for the estimation of the FRF amplitude under any excitation frequency involved in the problem.

4. Uncertainties observed in the PEHs

This section presents the most relevant results obtained in the experimental test. As it was discussed in Section 2.2, three analyses are independently conducted in order to identify and rank the sources of uncertainty. These analyses evaluate: (1) the repeatability of the FRF measured, (2) the sensitivity of the mounting process over the FRF, and (3) the FRF of several PEHs with identical nominal values and their respective comparison with the numerical predictions.

4.1. Consistency of the measurements (Test 1)

The first step in any experimental setup deals with the identification of the confidence level involved in the FRF identification. In that sense, an adequate experimental setup is fundamental to expect high levels of repeatability or minor dispersion in the measurements. The measurement dispersion comes from the fact that it is impossible to have absolute control over an experiment; e.g., presence of electric noise in sensors, friction between parts, non-ideal boundary conditions, among others, could affect the quality of the measurement and should be carefully quantified and reported. For this particular research, an extensive study of repeatability is performed in order to identify the baseline dispersion for the FRFs. The term baseline dispersion is used here to denote the intrinsic variability in the FRF identification, whereby it could be understood as an aleatoric variation. Note that in Section 2.2 it was argued that the instrumental noise could be neglected since it has not influence on the FRF identified. In other words, a single identification of a FRF it is considered free of errors (the noise is not significant compared to the PEH response). However, repeated identifications of the FRF show variations that should be characterized.

The FRF of each PEH is estimated by performing 100 independent measurements, which are then used to obtain the mean values at difference frequencies and their respective standard deviations. By example, Fig. 5 presents the FRF of the PEHs identified as PZT-A-05 and PZT-B-06, the figure shows the 100 measurements (in grey), while the mean value and the standard deviation for a given frequencies are presented in a black solid line and error bars, respectively. For the sake of brevity, results of others PEHs tested are not presented since they showed a similar trend. As it is expected, Model B has a lower natural frequency when it is compared to the natural frequency of Model A. Note that both models have the same nominal width b but Model A is shorter (lower L) and indeed stiffer. Additionally, the FRF of Model B has a peak significantly greater than Model A (almost twice the peak value of Model A) that is also explained by the difference in the length [13]. However, the interesting result here is related to the dispersion identified (error bars in Fig. 5), where it is observed a small coefficient of variation (CV) for both cases indicating an important level of repeatability. In general, the CV is lower than 2% except for

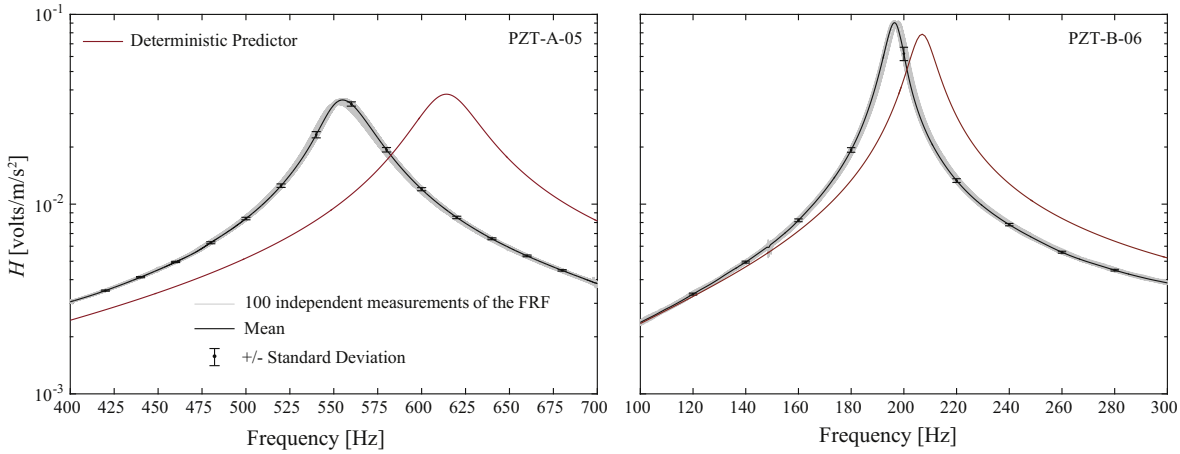

Fig. 5. 100 measurements of the FRF, mean value, and its standard deviation. Left figure corresponds to Model A and right figure to Model B.

frequencies close to resonance, where it is possible to observe CV up to 4% and 7% for Model A and B, respectively. These variations are independent of the instrumental noise and the excitation amplitude since they are valid for the excitation range that enforce a linear behaviour. Additionally, the measurements are compared with the deterministic prediction presented in Section 3.1 (red solid line in Fig. 5), where it is possible to observe important differences in the estimation of the fundamental frequency.

4.2. Uncertainties associated to the PEH mounting (Test 2)

In a previous work [15], it was identified that the FRF (more specifically the fundamental frequency) is sensitive to small changes in the PEH length. The effective length of the PEH is defined (please refer to Fig. 2) as the length of the PEH that is in cantilever, as a result, this length depends on the mounting process and the quality of the fixing constrain. The question that arise here is how different is the FRF when a PEH is installed, uninstalled, and reinstalled again. Moreover, it is necessary to identify how significant is this variation compared to the variations obtained in Section 4.1.

In particular, the FRF of each PEHs studied is identified after repeating the installation process. The PEH is installed and uninstalled 5 times, after each installation the FRF is identified by using 10 independent measurements. Results are presented in Fig. 6 keeping the same format employed in Fig. 5: the black solid line represents the expected value for a given frequency, the grey solid line represents each individual measurement while the error bars indicate the dispersion by accounting the standard deviation.

Although several PEHs are tested, the results presented here correspond to the same PEHs used to obtain Fig. 5, which allows a direct comparison between both testing conditions. Nonetheless, it is important to mention that the behaviour

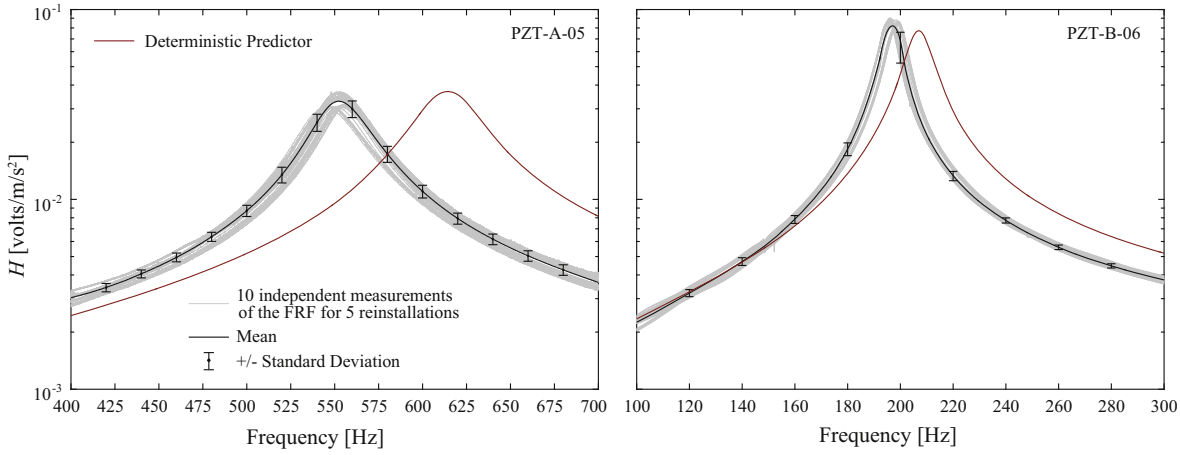

Fig. 6. Effect of the mounting process in the dispersion of the FRF. Each PEH is installed and uninstalled 5 times, for each installation the FRF is identified 10 times. Each measurement is presented in grey, the mean corresponds to the black line while the error bar indicates the standard deviation.

showed in Fig. 6 is representative of the rest of the PEHs tested. Here, the CV has the same trend previously observed, it increases close to resonance and decreases out of it, but its value is considerably higher, reaching CVs up to 11% and 18% for Model A and B, respectively. Note that these CVs are close to be 3 times the CVs identified as the baseline. Similar to the previous case, the measurements are also compared with the deterministic prediction (red solid line in Fig. 6), where it is possible to observe again an important frequency mismatch.

4.3. Uncertainties associated to the manufacturing process (Test 3)

This section identifies the variation in the FRF of PEHs that share the same nominal characteristics. In this section, all PEHs corresponding to model A and B are compared between them in order to identify the real dispersion on the manufacturing tolerance associated to the material properties and the geometry. Here, 20 PEHs corresponding to model A and 10 corresponding to model B are tested. The FRF of each single PEH is identified through 20 independent measurements and the results are presented in Fig. 7. Following the previous figure's legend, the black solid line represents the expected value for a given frequency while each grey solid line represents a single measurement of the FRF. Since 20 PEHs are tested and each one is tested 20 times, the total number of solid grey lines for Model A is 400. On the other hand, the Model B presents only 200 measurements since the total number of PEHs is 10. Here, the error bars represent the standard deviation of the measurement for a given excitation frequency (as it is used in previous cases). Results are very interesting since the CVs observed are considerably greater than previous cases (at least 4 times higher than test 2), reaching in some cases values up to 60%. Additionally, the whole set of measurements can be compared with the deterministic prediction (red solid line in Fig. 7). Here an interesting result is found since the nominal characteristics of the harvester seems to overestimate the fundamental frequency, i.e., the most part of the experimentally identified FRFs are centred at the left of the nominal prediction (deterministic prediction). More details on this issue are offered in Section 4.4 when the deterministic and stochastic predictions are compared with all the measurements performed.

To establish a more comprehensive comparison it is decided to present a new figure with the CV observed in the three tests conducted. In that sense, Fig. 8 shows the variation of the CV respect to the excitation frequency for the cases studied. The blue line indicates the CV for test 1, representing the level of basal uncertainty involved in the experiment. The red line indicates the CV for test 2, which is representative of the variation introduced by the basal uncertainty together with the variation introduced by the clamping condition at the fixed end of the PEH. On the other hand, the yellow line indicates the CVs identified in test 3, corresponding to variations introduced by the basal uncertainty, clapping condition and variations in the geometric parameters together with variations presented in the electromechanical properties of each PEH. Note that the area between yellow and red lines can be interpreted as the uncertainties introduced only by variations in geometry and electromechanical properties of the PEH. However, the geometric parameters of the PEHs tested were fully identified in Table 2, where it is possible to observe coefficient of variations lower than 2.6%, suggesting that the uncertainties identified in Fig. 8 can be attributed primarily to the electromechanical characteristics of the PEH. In this sense, it is important to note that any variation in the external conditions of the harvester, e.g., different electrical resistors or changes from parallel to serial connection of the piezoelectric layers, will not significantly affect the uncertainties identified. Note that changing the previous conditions affects the amplitude of the FRF, however, the only amplitude-dependent uncertainty is related to the instrumental noise, which in this case could be neglected based on the argument presented in Section 2.2.

The results found here are completely in agreement with the conclusion established by Ruiz and Meruane [15], in the sense that the electromechanical properties of the harvester are the most important parameters to be controlled in order

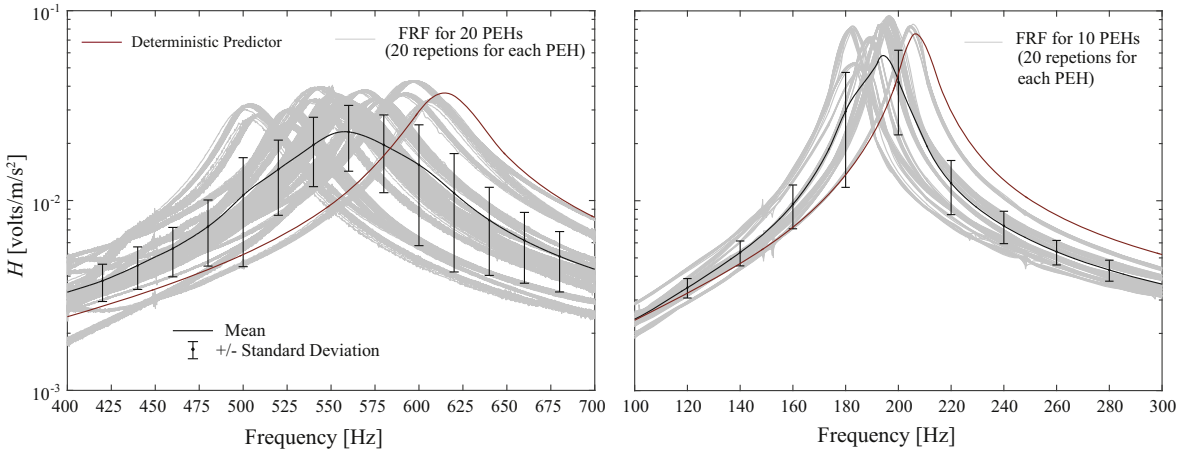

Fig. 7. FRFs for all PEH tested. Left figure presents 20 FRF of each PEH identified as model A, the mean and standard deviations are also presented. Right figure presents 20 FRF of each PEH identified as model B, the mean and standard deviations are also presented.

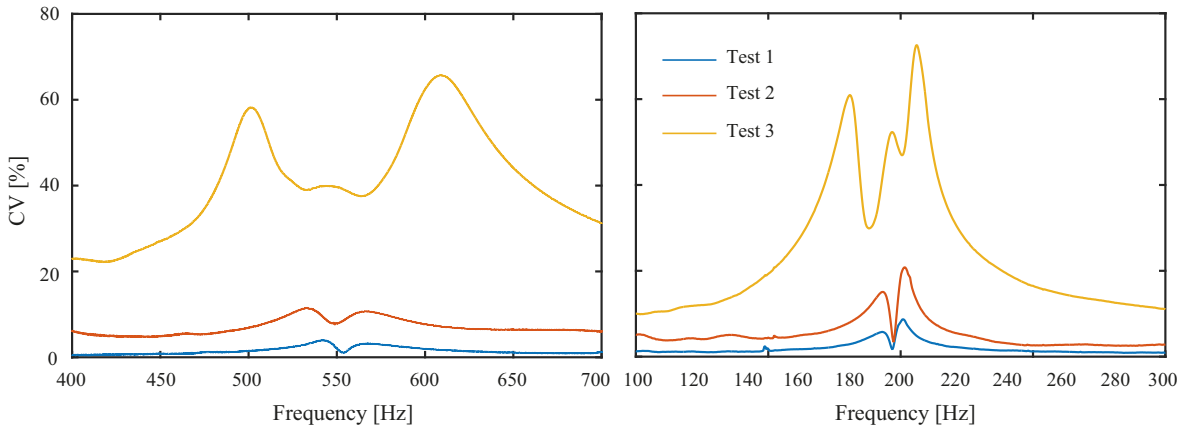

Fig. 8. Coefficient of variations (CV) of the FRF amplitude given a known excitation frequency.

to increase the predictability of the FRF. Unfortunately, given the conditions of the experimental setup it is not straightforward to identify which of the electromechanical properties contributed the most in the CV. Nevertheless, some advanced stochastic techniques can be applied here to address this topic, by example, employing Bayesian updating techniques [22]. Although those techniques are well-known, it is required an important level of expertise in order to properly identify the probabilistic density function associated to each electromechanical parameter that leads to the variations observed in the experiments. This procedure is part of the ongoing research, reason why it is not included here. Additionally, it is considered that further details on this topic can deviate the attention of the reader from the scope of the present work.

As additional comment, it is important to remark the meaning of the CV identified in the experimental tests. The CV presented, in particular from Figs. 5–8, indicates the expected variation of the FRF amplitude for a given excitation frequency. In other words, it is the variation expected if the excitation frequency is known, which is representative of a narrow band excitation. If it is the case (known narrow band excitation process), the results evidence the low likelihood to select a PEH (based in its nominal values) with a fundamental frequency such that a resonance condition could be enforced. As a result, there is a high likelihood to obtain an electrical power considerably lower than the nominal value estimated.

A different situation occurs for broadband excitation process since it is very likely to excite the fundamental frequency of the PEH. In this case, the relevant information, from the design point of view, corresponds to the maximum value of the FRF ($H_{\max}$) and its location (fundamental frequency ω_{fun}). Tables 3 and 4 present the mean and deviation of those parameters for results showed in Figs. 5–7. Here, it is identified that basal uncertainties (test 1) induce changes lower than 1% in the mean value of $H_{\max}$ and ω_{fun}. These values are increased when the clapping condition is changed (test 2). However, the variation of the fundamental frequency still being lower than 1% of its mean value, while the variation in $H_{\max}$ rises to 6.5% and 3.1% for

Table 3
Maximum amplitude of the FRF for the tests conducted. Mean values, standard deviations and coefficient of variations are reported. Units correspond to [volts/m/s^2]. Coefficient of variation is reported in parenthesis.

	Model A		Model B	
	Mean of $H_{\max}$	Standard deviation	Mean of $H_{\max}$	Standard deviation
Test 1	0.0357	0.0003 (0.8%)	0.0912	0.0008 (0.9%)
Test 2	0.0337	0.0022 (6.5%)	0.0868	0.0027 (3.1%)
Test 3	0.0334	0.0040 (12.0%)	0.0830	0.0122 (14.7%)

Table 4
Fundamental frequency for PEHs tested. Mean values, standard deviations and coefficient of variations are reported. Units correspond to [Hz]. Coefficient of variation is reported in parenthesis.

	Model A		Model B	
	Mean of ω_{fun}	Standard deviation	Mean of ω_{fun}	Standard deviation
Test 1	554.94	1.09 (0.2%)	196.47	0.49 (0.2%)
Test 2	551.91	3.01 (0.5%)	196.91	1.24 (0.6%)
Test 3	556.10	26.75 (4.8%)	193.11	6.58 (3.4%)

Model A and B, respectively. When all PEHs are taken into account (test 3), the dispersion of $H_{\max}$ takes values of at least 10% while the variations in ω_{fun} are lower than 5%. Results reveal that although small CVs are expected for ω_{fun} (CV < 5%), they introduce significant variations (CV greater than 10%) in the maximum value of the FRF. In particular, the CV of $H_{\max}$ is between 2.5 and 4 times the CV of ω_{fun} for the cases studied. Nonetheless, the variations related to the output power assuming a broadband excitation are considerable lower than the variations associated to a narrow-band excitation. Effect that occurs since the amplitude of the FRF is very sensitive to changes in the excitation frequency, especially when the excitation frequency is close to ω_{fun}.

4.4. Predictions vs observed uncertainties

The interest of this section is to compare the FRF measurements with the confidence intervals predicted by the numerical method described in Section 3. This prediction requires that all parameters involved in the predictive model be defined by a PDF. The geometric characteristics of the harvester are considered lognormal distributions; specifically the values presented in Table 2 are used as median and coefficient of variation for the thickness and width. The length presented in Table 2 it is not used here since it represents the total length of the PEH rather than the cantilever length of the beam (called effective length in Fig. 2). The median effective length used here corresponds to 23.5 mm and 40 mm, for model A and B, respectively. Based on measurements, their respective coefficients of variation are assumed equal to 2%. The electromechanical parameters s_{11}^{E}, d_{31}, ε_{33}^{T}, and ρ_p are assumed as normal distributions, with mean values equal to nominal values presented in Table 1, and with a coefficient of variation equal of 20% (as it is reported by the manufacturer). Here, it is important to note that there is not information about the substructure density ρ_s and elastic modulus E_s, reason why it is decided to match the probabilistic model of these properties with the mechanical properties of the piezoelectric layers. The selection of the normal PDF is based on the principle of information entropy, which establishes that normal PDFs are the most conservative probabilistic model or the model that introduces the greatest amount of uncertainty to the analysis. This principle is valid only when the known parameters correspond to the mean and the standard deviation of a random variable [21].

The comparison between measurements and predictions are presented in Fig. 9. There, it is possible to observe the measurements in grey, the dotted lines correspond to the exceedance probability equal to 90% (P_o = 0.9) and 10% (P_o = 0.1), the black solid line corresponds to the expected value estimated by the stochastic predictor, while the red solid line incorporates the deterministic prediction. Here, it is important to recall Eq. (5) which defines the exceedance probability, in that sense, the area between the dotted lines represents an interval confidence equal to 80%. The first interesting observation is that the measurements lie inside the interval confidence area, which shows the capability of the numerical procedure to estimate the possible location of the actual FRF. However, the fundamental frequency estimated by the deterministic and stochastic predictors is higher than the mean fundamental frequency observed, the prediction estimates 625 Hz for model A and 200 Hz for model B while the fundamental frequency observed has a mean of 550 Hz in model A and 195 Hz in model B. This bias identified between mean values of prediction and measurement indicates that the nominal values employed in the predictions are not completely accurate. Additionally, it is observed that the dispersion used in the predictive model is considerable greater than the actual dispersion of each set of PEHs. As it was mentioned before, part of the ongoing work is focused in the identification of the dispersion employed in the predictive model such that the measured FRFs are just bounded by the exceedance probability curves. Note that this problem could be tackled in two different directions: (i) updating the uncer-

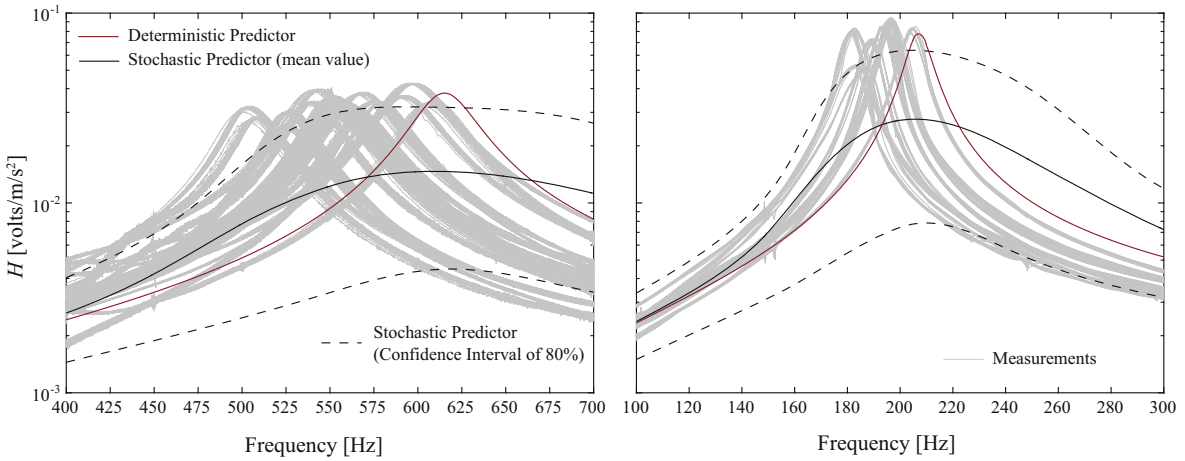

Fig. 9. Experimental FRFs together with the interval confidence predicted by the numerical approach presented in Section 3.

tainties using the whole set of PEHs to increase the predictability of a new PEH manufactured or (ii) updating the uncertainties using several measurements of a single PEH to increase the predictability of its response in future events.

5. Conclusions

An experimental setup capable to determine the FRF of PEHs was developed and successfully tested, specifically in the uncertainty quantification related to: basal variations, installation process, manufacturing tolerance and electromechanical properties of the materials. The experimental setup facilitates the identification of FRFs in PEHs by: (1) automatic imposition of recursive sweep excitations and (2) properly designing a quick install/release mounting clamp.

Two PEH models were tested, Model A and B, both with different nominal characteristics. A set of 20 Model A and 10 Model B harvesters were tested. Each measurement was repeated 100 times in order decrease statistic errors where the results were used to validate the uncertainty propagation procedure previously proposed by the authors [15].

Since multiple measures were conducted to each single PEH, its FRF were reported employing mean values and their respective coefficients of variation. The maximum basal variation associated to the FRF amplitude was reported as 4% and 7% of the mean value for Model A and Model B, respectively. The installation process revealed an increment in the level of dispersion presented in the FRF; by example, a PEH after being installed, uninstalled and reinstalled again multiples times, presents variations in the FRF in the order of 11% for Model A and 18% for Model B, both numbers referred to their respective mean value. When the whole set of PEHs were studied, the variations in the FRF amplitude was increased notoriously, showing coefficient of variations up to 60% in both PEH models. However, the coefficient of variation associated to the fundamental frequency is lower than 5%, indicating a high sensitivity of the fundamental frequency in the interval confidence associated to the FRF amplitude.

In general, all FRFs identified (for all cases studied) lie inside the confidence interval predicted by the numerical procedure employed. The variation found in the experimental identification of FRFs (for the same harvester model) justify the use and show the adequacy of the numerical procedure employed here to propagate and quantify the uncertainties in PEHs. The experimental results obtained could be also used to calibrate a predictive model adopting, by example, a Bayesian updating technique, which is part of the ongoing research.

Acknowledgments

This research is supported by the Comisión Nacional de Investigación Científica y Tecnológica de Chile through the project CONICYT/FONDECYT/3160491.

Appendix A

This section explicitly presents the expressions that relate each term of FRF presented in Eq. (3) with the characteristics of a bimorph PEH. In particular, $\mathbf{C}_{eq}$ and $\mathbf{K}_{eq}$ are $M-$by$-M$ diagonal matrices defined as

$$\begin{aligned}\mathbf{C}_{eq} &= diag[\,2\xi_1\omega_{n_1} \quad 2\xi_1\omega_{n_2} \quad \cdots \quad 2\xi_M\omega_{n_M}\,]\\ \mathbf{K}_{eq} &= diag[\,\omega_{n_1}^2 \quad \omega_{n_2}^2 \quad \cdots \quad \omega_{n_M}^2\,]\end{aligned} \tag{9}$$

while $\boldsymbol{\varphi}$, $\boldsymbol{\chi}$, and $\mathbf{r}$ are defined as the following column vectors

$$\begin{aligned}\boldsymbol{\varphi} &= [\,\varphi_1 \quad \varphi_2 \quad \cdots \quad \varphi_M\,]^T\\ \boldsymbol{\chi} &= [\,\chi_1 \quad \chi_2 \quad \cdots \quad \chi_M\,]^T\\ \mathbf{r} &= [\,r_1 \quad r_2 \quad \cdots \quad r_M\,]^T\end{aligned} \tag{10}$$

Ultimately, the modal characteristics ξ_m (damping ratio), ω_{n_m} (natural frequency), φ_m (mechanical coupling term), χ_m (electrical coupling term), and r_m (mechanical forcing amplification due to inertial effect); could be related to the PEH characteristics $\boldsymbol{\theta}$ following the procedure introduced by [12]. The procedure is based on a modal expansion of M eigenfunctions of the form:

$$\phi_m(x) = C_r\left[\cos\left(\frac{\lambda_m x}{L}\right) - \cosh\left(\frac{\lambda_m x}{L}\right) + \sigma_i\left(sin\left(\frac{\lambda_m x}{L}\right) - sinh\left(\frac{\lambda_m x}{L}\right)\right)\right] \tag{11}$$

where L corresponds to the length of the PEH, σ_m is defined as

$$\sigma_m = \frac{sin(\lambda_m) - sinh(\lambda_m)}{cos(\lambda_m) + cosh(\lambda_m)} \tag{12}$$

while λ_m corresponds to the roots of the following characteristic equation

$$1 + \cos(\lambda)\cosh(\lambda) = 0 \tag{13}$$

Finally, the normalization constant C_r is defined such that the following condition is enforced

$$\int_0^L \phi_s(x) m \phi_p(x) dx = \delta_{sp} \quad \text{for} \quad \begin{matrix} \delta_{sp} = 1 \ \ if \ \ s = p \\ \delta_{sp} = 0 \ \ if \ \ s \neq p \end{matrix} \tag{14}$$

After defining the eigenfunctions, the modal characteristics of the PEH can be defined as:

$$\omega_{n_m} = \lambda_m^2 \sqrt{\frac{EI}{m_o L^4}} \tag{15}$$

$$\begin{aligned} \varphi_m &= -\frac{d_{31}}{s_{11}^E} \frac{h_p (h_p + h_s)}{\varepsilon_{33}^S L} \frac{d\phi_m(x)}{dx}\bigg|_{x=L} \quad (series) \\ \varphi_m &= -\frac{d_{31}}{s_{11}^E} \frac{h_p (h_p + h_s)}{2\,\varepsilon_{33}^S L} \frac{d\phi_m(x)}{dx}\bigg|_{x=L} \quad (parallel) \end{aligned} \tag{16}$$

$$\begin{aligned} \chi_m &= -\frac{d_{31}}{s_{11}^E} \frac{b}{2\,h_p} \left(\frac{h_s^2}{4} - \left(h_p + \frac{h_s}{2} \right)^2 \right) \frac{d\phi_m(x)}{dx}\bigg|_{x=L} \quad (series) \\ \chi_m &= -\frac{d_{31}}{s_{11}^E} \frac{b}{h_p} \left(\frac{h_s^2}{4} - \left(h_p + \frac{h_s}{2} \right)^2 \right) \frac{d\phi_m(x)}{dx}\bigg|_{x=L} \quad (parallel) \end{aligned} \tag{17}$$

$$r_m = -m_o \int_0^L \phi_m(x) dx \tag{18}$$

$$\begin{aligned} k_{pzt} &= \frac{2\,h_p}{R\left(\varepsilon_{33}^T - \frac{d_{31}^2}{s_{11}^E}\right) b L} \quad (series) \\ k_{pzt} &= \frac{h_p}{2\,R\left(\varepsilon_{33}^T - \frac{d_{31}^2}{s_{11}^E}\right) b L} \quad (parallel) \end{aligned} \tag{19}$$

In previous equations, m_o denotes the mass per unit of length, while EI corresponds to the equivalent bending stiffness of the PEH given by

$$EI = \frac{2b}{3} \left[E_s \frac{h_s^3}{8} + \frac{1}{s_{11}^E} \left(\left(h_p + \frac{h_s}{2} \right)^3 - \frac{h_s^3}{8} \right) \right] \tag{20}$$

As the PEH of interest is a bimorph type (two piezoelectric layers are bonded to a main structure), then the electrodes of each piezoelectric layer can be connected in series or in parallel depending whether a larger voltage or current is desired, respectively.

References

[1] A. Erturk, D.J. Inman, Piezoelectric Energy Harvesting, John Wiley & Sons, 2011.
[2] H.A. Sodano, D.J. Inman, G. Park, A review of power harvesting from vibration using piezoelectric materials, Shock Vib. Dig. 36 (3) (2004) 197–205.
[3] S. Roundy, P.K. Wright, J. Rabaey, A study of low level vibrations as a power source for wireless sensor nodes, Comput. Commun. 26 (11) (2003) 1131–1144.
[4] A. Erturk, D.J. Inman, A distributed parameter electromechanical model for cantilevered piezoelectric energy harvesters, J. Vib. Acoust. Trans. ASME 130 (4) (2008).
[5] H.A. Sodano, G. Park, D.J. Inman, Estimation of electric charge output for piezoelectric energy harvesting, Strain 40 (2) (2004) 49–58.
[6] V. Meruane, K. Pichara, A broadband vibration-based energy harvester using an array of piezoelectric beams connected by springs, Shock Vib. 2016 (2015).
[7] H.C. Lin, P.H. Wu, I.C. Lien, Y.C. Shu, Analysis of an array of piezoelectric energy harvesters connected in series, Smart Mater. Struct. 22 (9) (2013).
[8] A. Lei et al., MEMS-based thick film PZT vibrational energy harvester. in: Micro electro mechanical systems (MEMS), 2011 IEEE 24th international conference on, 2011, pp. 125–128.
[9] Y.B. Jeon, R. Sood, J.-H. Jeong, S.-G. Kim, MEMS power generator with transverse mode thin film PZT, Sens. Actuators Phys. 122 (1) (2005) 16–22.
[10] N.E. DuToit, B.L. Wardle, S. Kim, Design considerations for MEMS-scale piezoelectric mechanical vibration energy harvesters, J. Integr. Ferroelectr. 71 (2005) 121–160.
[11] G.D. Szarka, B.H. Stark, S.G. Burrow, Review of power conditioning for kinetic energy harvesting systems, IEEE Trans. Power Electron. 27 (2) (2012) 803–815.
[12] A. Erturk, D.J. Inman, An experimentally validated bimorph cantilever model for piezoelectric energy harvesting from base excitations, Smart Mater. Struct. 18 (2) (2009) 025009.
[13] C.D.M. Junior, A. Erturk, D.J. Inman, An electromechanical finite element model for piezoelectric energy harvester plates, J. Sound Vib. 327 (1) (2009) 9–25.
[14] V.R. Franco, P.S. Varoto, Parameter uncertainties in the design and optimization of cantilever piezoelectric energy harvesters, Mech. Syst. Signal Process. 93 (2017) 593–609.
[15] R.O. Ruiz, V. Meruane, Uncertainties propagation and global sensitivity analysis of the frequency response function of piezoelectric energy harvesters, Smart Mater. Struct. 26 (6) (2017) 065003.
[16] Sinocera http://www.sinocera.net/, 2016.
[17] S. Leadenham, A. Erturk, Unified nonlinear electroelastic dynamics of a bimorph piezoelectric cantilever for energy harvesting, sensing, and actuation, Nonlinear Dyn. 79 (3) (2015) 1727–1743.

[18] Y. Yang, D. Upadrashta, Modeling of geometric, material and damping nonlinearities in piezoelectric energy harvesters, Nonlinear Dyn. 84 (4) (2016) 2487–2504.
[19] S.C. Stanton, A. Erturk, B.P. Mann, E.H. Dowell, D.J. Inman, Nonlinear nonconservative behavior and modeling of piezoelectric energy harvesters including proof mass effects, J. Intell. Mater. Syst. Struct. 23 (2) (2012) 183–199.
[20] S.K. Au, J.L. Beck, A new adaptive importance sampling scheme for reliability calculations, Struct. Saf. 21 (2) (1999) 135–158.
[21] R.D. Rosenkrantz, E.T. Jaynes, Papers on Probability, Statistics and Statistical Physics, Springer Science & Business Media, 2012.
[22] J.L. Beck, A.A. Taflanidis, Prior and posterior robust stochastic predictions for dynamical systems using probability logic, Int. J. Uncertain. Quantif. 3 (4) (2013) 271–288.